Contents

8. Calculation of Sheath and Wake Structure about a Pillbox-Shaped Spacecraft in a Flowing Plasma

Lee W. Parker
Lee W. Parker, Inc.
Concord, Mass.

Abstract

This paper is concerned with a computer program used for studies of the disturbed zones around bodies in flowing plasmas, particularly spacecraft and their associated sheaths and wakes. The program solves a coupled Poisson-Vlasov system of nonlinear partial-differential-integral equations to obtain distributions of electric potential and ion and electron density about a finite-length cylinder in a plasma flow at arbitrary ion Mach numbers. Using the author's "inside-out method"[6] which follows ion and electron trajectories backward to their origin at the body surface or in the undisturbed plasma, together with a special iteration algorithm for self-consistency, the program takes into account the particle thermal motions with relatively few simplifying assumptions. The approach is applicable to a larger range of parameters than other available approaches. In sample calculations, bodies up to 100 Debye lengths in radius are treated, that is, larger than any previously treated realistically. Applications are made to in-situ satellite experiments.

1. INTRODUCTION

The problem of theoretically calculating the structure of the disturbed plasma (frequently referring to the wake and/or sheath) around a moving body in space involves the solution of a complicated system of coupled nonlinear partial differential/integral equations.[1] The equations consist of the Vlasov (collisionless Boltzmann) equations for the ions and electrons, and the Poisson equation relating the electric field to the distributions of ions and electrons. The difficulty is essentially a numerical one because analytic solutions are not possible (for cases of interest), and there is no unique approach. In cases of stationary bodies,[2-5] as well as moving bodies (theoretical references cited by Parker[1]), combinations of numerical techniques (finite differences, iteration, quadratures, etc.) are required for treating various parts of the problem. For either stationary or moving bodies, the choices of techniques and their use to achieve consistent solutions for any given set of physical parameters (defining body and plasma) have never been obvious. Innovations are frequently required. The purpose of this paper is to present a technique suitable for a pillbox-shaped body (with emphasis on the wake),[1] which appears to be reasonably successful over a large range of the physical parameters, and to present sample solutions including applications to in-situ spacecraft data. The pillbox problem is illustrated schematically in Figure 1.

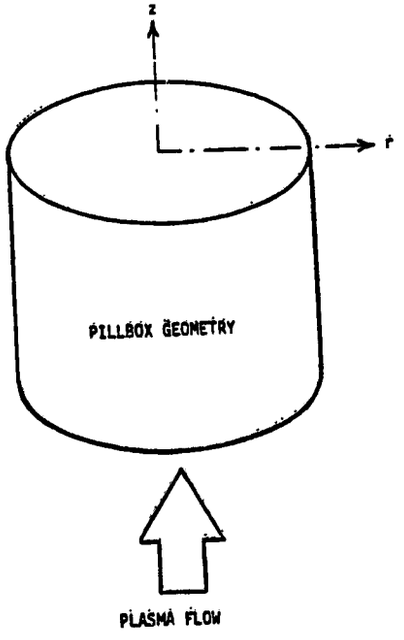

Figure 1. Spacecraft and Plasma-Flow Geometry

Various approaches which have been used for this type of problem are summarized by Parker.[1] In all such calculations, simplifying assumptions are made. The customary ones are:

(1) Collisions negligible (but extensions of Parker's collisional theory[4] may be feasible for the wake problem).

(2) Geomagnetic field negligible.

(3) Simplified geometry (use of various types of symmetries).

(4) Simplified surface reactions (usually, charged particles are neutralized).

(5) Prescribed surface emission (usually none, but simplified photoelectron, backscattered-electron, and secondary-electron emission are includable).

(6) Conducting body (usually perfectly conducting, but finite conductivities are includable).

(7) Steady state.

These assumptions may be questioned (for example the neglect of time-dependent phenomena), but they may be at least partially relaxed by employing known techniques to generalize the calculations. In the interest of achieving reasonably economical calculations within the limits of available computers, the above assumptions in their usual form are adopted in the present work.

The techniques and computer program described by Parker[1] have been developed to solve the coupled Poisson-Vlasov system of equations to obtain distributions of ion and electron density, and potential, about three-dimensional bodies (with axial symmetry about the direction of plasma flow). The method involves the use of a numerical grid or mesh of discrete points in space, with the potential and density distributions defined at these points. The Poisson and Vlasov equations are represented in finite-difference form at the grid points. A sample of such a discretization in r-z space is shown in Figure 2. Here the points represent circular rings about the z-axis. Associated with each point is a volume, in the form of a cylinder for points along the axis, and in the form of a torus of rectangular cross-section for all other points.

For the pillbox problem of Figure 1, the grid used has the form shown in Figure 3. The spacecraft surface is shown by a heavy outline in the interior of the grid. The surface of the pillbox coincides with certain rows and columns of grid points as shown. Here, the grid points are unequally spaced, so that a higher density of points can be used near the spacecraft surface and a lower density further away. This allows a given number of grid points to be used efficiently. The potentials at points on the surface can vary arbitrarily; the potential distribution shown corresponds to one part of the surface being at one potential (the "probe") while the remainder is at another potential. The surface can consist of portions with arbitrarily assigned conductivity and emission characteristics. The actual number of grid points used was of the order of hundreds, rather than tens

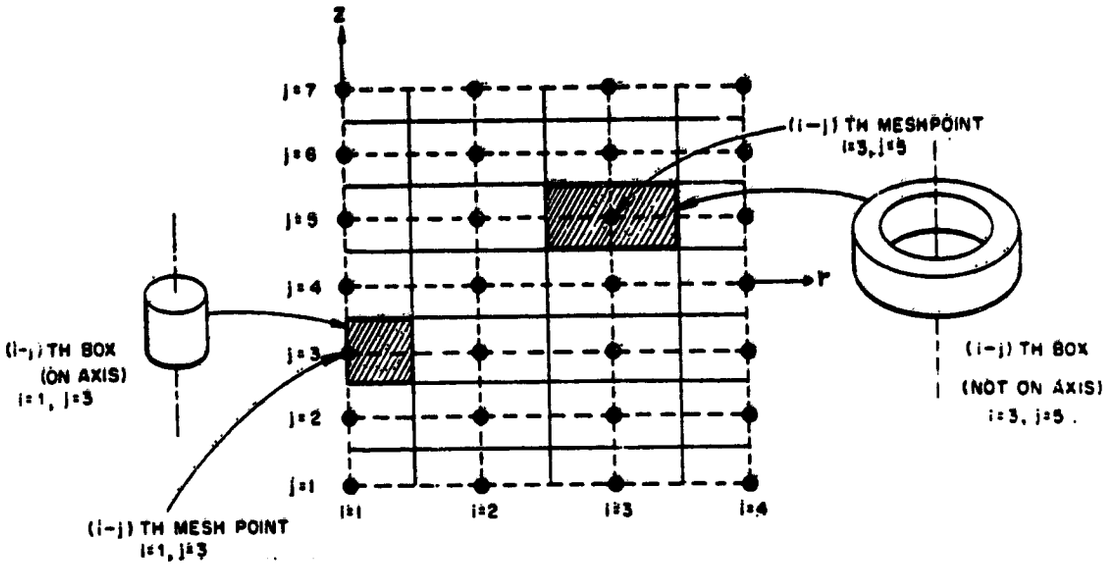

Figure 2. Discretization in r-z Space

as illustrated.) The shaded areas surrounding grid points are the cross-sections of toroidal volumes as in Figure 2. At the outer boundary of the grid, one must represent numerically the boundary condition at infinity, namely, such that the potential vanish and the velocity distribution be the unperturbed one. This boundary must be sufficiently far out to represent the outer condition accurately. It turns out to be more efficient to use a "floating" rather than a "fixed" condition on the potential (Section 3).

While the present problem is axially symmetric, it can be generalized to three dimensions as follows. The grid in Figure 3 consists of points in r-z space, and the associated volumes are tori. The generalization would consist of including the azimuthal variation by adding an azimuthal angle θ to the coordinate system. The discretization in θ would consist of having a number of azimuthal planes in r and z, each labeled by a given value of θ. Thus, for example, the r-z plane of Figure 3 would be characterized by a given value of θ. The volumes associated with the grid points would then be pie-shaped.

In the next section (Section 2) the "inside-out" method for evaluating particle fluxes and densities (solving the "Vlasov problem"), developed by the author[6] in 1964, will be discussed, with reference to the grid of Figure 3. In this method the ion and electron trajectories are followed backward in time, from the point in space at which it is desired to know the velocity distribution, to the source of the

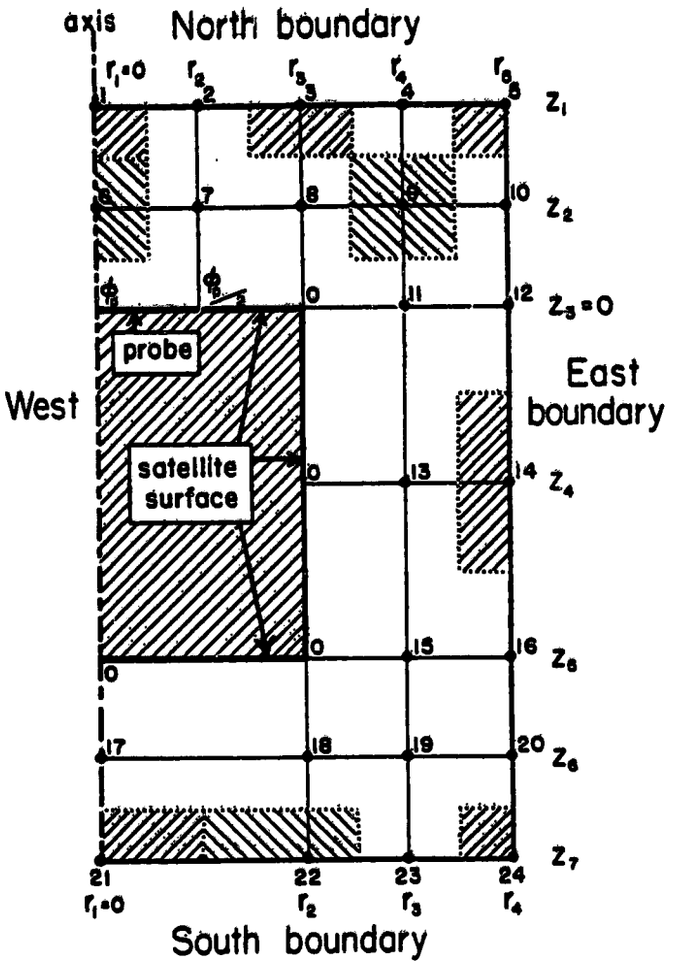

Figure 3. Difference Equation Grid

particles in the undisturbed plasma or at the surface, where the distributions are known. Figure 4, referred to again in the next section, illustrates schematically how a trajectory is traced backward from any point P and is found either to reach the body surface or "infinity" at the boundary of the grid. (The point P is usually but not necessarily one of the spatial grid points; it can also be a surface point.) The "delta-factor" δ_{ijk} is a cutoff function, and i, j, and k are indices associated with one of the trajectories used to evaluate density or flux as discussed in the next section. The case illustrated is for contributions from the ambient plasma; for contributions from the surface, the values of δ (zero and unity) are interchanged.

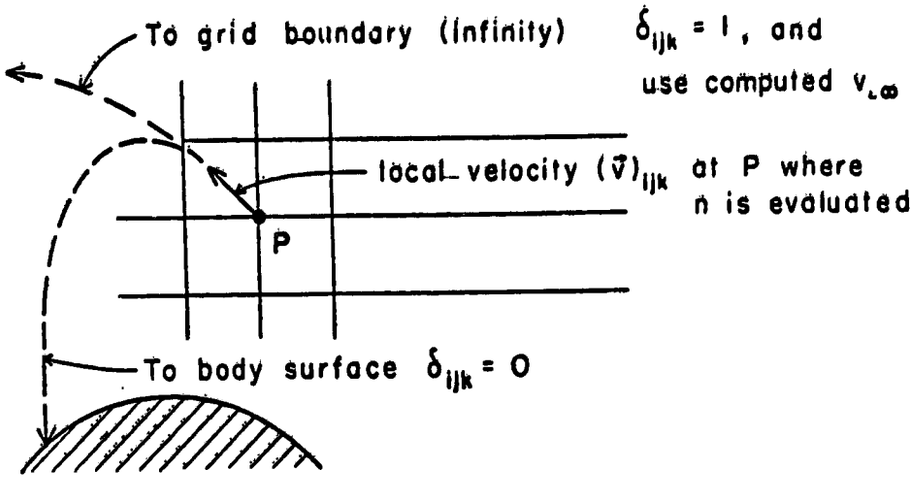

Evaluation of δ_{ijk} for (i,j,k)-th trajectory by following (reversible) trajectories backward in time.

Figure 4. Basis of the Inside-Out Method

Figure 5 illustrates the four possible types of trajectories which can contribute to the particle density at a point. These are Types 1, 2, 3, and 4, so-named by Parker[4] and defined as follows:

Type 1

One-way trajectories, going from infinity to the surface, or from the surface to infinity.

Type 2

Two-way trajectories from infinity, which come in, pass through a position at minimum distance from the body surface, and go out again.

Type 3

Two-way trajectories from the body surface, which go out, pass through a position at maximum distance from the body surface, and come in again.

Type 4

Closed or nearly-closed trajectories which orbit about the body indefinitely. These can only be populated and depopulated by collisions, which are neglected in the present work. An analysis of the effects of collisions on Type-4 trajectories has been performed by Parker.[4]

It should be noted that contributions to surface fluxes can be comprised only of Type-1 and Type-3 trajectories, while all four types contribute to space charge.

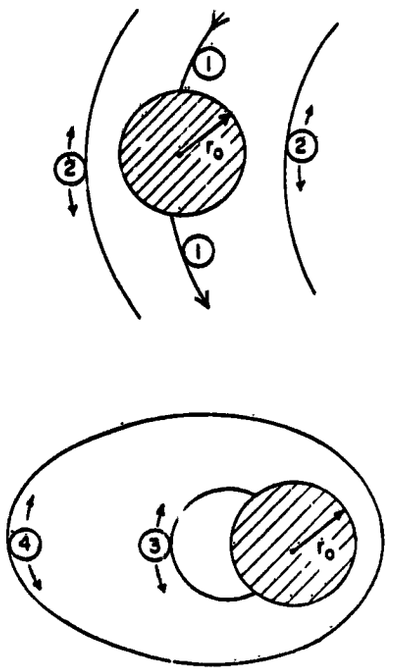

Figure 5. Types of Orbits

In Section 3 the "Poisson Problem" is discussed, where the electric field (potential distribution) is computed with the ion and electron densities considered known.. On the other hand, the "Vlasov Problem" (Section 2) involves computation of the ion and electron densities with the field considered known. Hence, since neither the field nor the particle densities are known initially, the Poisson and Vlasov problems must be solved simultaneously.

An iteration method may be used for computing self-consistent charged-particle and potential distributions. This is herein referred to as the "Poisson-Vlasov iteration." Two principal options are employed for this procedure in the present program. In one of the options, the "charge-density" option, the space charge is initially and arbitrarily assumed to be zero. For this case, one obtains the Laplace (space-charge-less) electric field from the Poisson problem. This is the "zero-order" potential distribution, which becomes input to the Vlasov problem. The resulting solution of the Vlasov problem yields the ion and electron densities at the grid points, which are combined to make "zero-order" charge densities. These become input to the next Poisson problem, which then yields the "first-order" potentials, and so on. In this procedure one usually "mixes" successive charge-density iterates to improve stability; otherwise, the process can "blow up." One can also mix potential iterates rather than densities if desired. The dependence

of the stability and convergence of the above procedure on the mixing parameter have been studied analytically by Parker[7] and Parker and Sullivan.[8] (No other analysis of this type has been published to the author's knowledge.) This (charge-density) option is most effective when the spatial region of interest is not too many Debye lengths across. The analysis shows that one can (probably always) choose a mixing parameter sufficiently small to ensure convergence, but at the expense of additional iterations.

In the other option, the "ion-density option," the ion density distribution alone is assumed initially. Initial guesses which can be employed include (1) zero ion density everywhere, (2) unit ion density (the ambient value) everywhere, and (3) the neutral ion density which obtains when there are no forces. Whichever choice is made for the initial guess is designated the "zero-order" ion density. Now if one can assume the electron density to be given by the Boltzmann factor $\exp(\phi)$, thus avoiding trajectory calculations for the electrons and affording computer economy, the Poisson equation may be solved, holding the ion densities fixed, but regarding both the potentials and the electron densities at the grid points as unknowns. This is a nonlinear problem, which is solvable by a modification of the relaxation procedure used for the "charge-density" option. The new procedure is an important advance since the iteration is not as sensitive (tending to blow up) for small Debye numbers as in the charge density option. Thus, very large bodies (in multiples of the Debye length) can be treated. This has been the method used to obtain the large-body results shown below.[1] Similar ideas have been used by Call[9] and Fournier,[10] but these workers have not treated large bodies.

The assumption that the electron density is given by the Boltzmann factor becomes invalid when the body surface potential is near zero, or when there is a potential barrier or "well" in the wake such that the wake potentials are more negative than the surface potential (causing electrons to be attracted to the surface rather than repelled from it). In this case it is still possible to use the ion-density option, with its large-body capability, provided that, within each "major" iteration cycle a "minor" iteration is carried out with the ion densities held fixed such that the electron densities are computed realistically by trajectory calculations, at least for points near the surface.

This latter technique is as yet in an experimental stage, but it seems promising in that it may produce solutions with reasonable costs for large-body problems; in such problems, the conventional Poisson-Vlasov iteration based on the charge-density option becomes expensive.[8] A disadvantage of the ion-density option, however, is that its convergence properties are not understood; therefore, its costs are difficult to predict. This is in contrast to the case of the charge-density option where an analysis is available.[8]

Before considering further details, we make here some general remarks concerning the method. Following this, the principal results will be summarized.

Briefly, the present approach[1] differs from those of Call[9] and Martin[11] by including both the ion and the electron thermal motions, whereas Call and Martin represent the distribution of ions by a cold beam and use an "outside-in" method.[1] The approach differs from that of Taylor[12] in that (1) it is applied to three-dimensional bodies whereas Taylor treats an infinitely-long "thick strip" of rectangular cross-section, and (2) the Poisson and Vlasov calculations are cycled until self-consistency is achieved, whereas Taylor's calculation is not self-consistent because it is terminated after the first cycle. The approach differs from that of Grabowski and Fischer[13] because they (1) assume that quasineutrality holds everywhere (an invalid assumption in the very near wake - see below and Section 5), and (2) apply their method to an infinitely-long cylinder. Differences with other methods are outlined in Parker.[1] The most similar calculation previously done was for an infinitely-long cylinder by Fournier,[10] using the inside-out method. The present author has used the method for two-electrode rocket-borne[7] and laboratory probe systems,[4] for the problem of a small probe in the sheath of a large electrode,[4] and most recently for the problem of the pillbox-shaped spacecraft.[1] The inside-out method was also used by Parker and Whipple[14] for the theory of a satellite flush-mounted probe.

Two major advances are represented by the present program, as opposed to previous approaches, particularly with regard to wakes of three-dimensional bodies:

(1) Thermal motions of ions as well as of electrons are treated realistically by following their trajectories in the electric field. (The ion and electron temperatures can be different.)

(2) The technique for achieving self-consistency is promising for large bodies many orders-of-magnitude larger than the Debye length (the Shuttle-Orbiter or the moon, for example).

Solutions may be obtained with reasonable amounts of computer time by judicious choices of grid points and other numerical parameters. The method can be extended to include an arbitrarily-shaped body (presently a body of revolution), electron emission from the surface, and differential charging when the surface consists of sections with different conductivity.

In Sections 2 and 3 some details of the techniques for the flux and density calculation ("Vlasov problem"), and for the Poisson calculation, are treated.

Sample calculational results are presented in Sections 4 and 5.

1.1 Summary of Principal Results

The principal results are as follows. In-situ experiments associated with the Ariel 1 and Explorer 31 satellites are modeled by a pillbox geometry. The Ariel 1 experiment observes distinct wake structures associated with the main body and a small external ion probe. Transverse profiles of electron current are measured at 5 main-body radii downstream. The two wake structures are similar in that they both show a below-ambient central core or peak within a depleted region of the order of the width of the main body. The theoretical results for the assumed values of the parameters associated with the experiment show no well-defined central core. They further show that all structure dies away beyond 6 or 8 radii downstream. A pronounced electrical focusing of ions in the wake of the highly-negative ion probe is predicted by the calculation, but this disturbance is confined to the relatively near wake and does not persist downstream. The filling of the wake in both cases by the plasma suggests a fluid-like bulk motion of the plasma. As one moves downstream with the plasma, the motion is at first radially inward. This is followed by a pile-up and a single "bounce" after which the motion is outward. Simultaneously, the disturbance becomes weak and dies away.

Two Explorer 31 cases are computed for different values of the ion Mach number (the other parameters remaining roughly comparable), and in both cases the body is several kT negative. In the case of the larger Mach number (3.4), the ion density in the near wake is below the corresponding electron density, and both are significantly below ambient. This is consistent with the traditional picture of wake structures with ion Mach numbers significantly above unity. In the case of the lower Mach number (1.1) the ion density in the near wake is above the corresponding electron density, and moreover the ion density is roughly ambient. This latter may seem unexpected, but is understandable on the basis of Langmuir-probe sheath theory: In the sheath of a slowly-moving negative probe the ion density should predominate over the electron density. This latter result is new in wake theory, and arises because low-Mach-number wakes with space charge have not been previously rigorously computed.

For the wake of a large body (100 Debye lengths in radius) in the form of a disk, the results show that quasineutrality is valid outside of a cone-shaped region in the very near wake, and is invalid within this region. Other features of the large-body wake structure include (1) a potential well in the near wake, and (2) a central core of approximately ambient density of both ions and electrons. This latter feature seems similar to that observed in the Ariel 1 experiment.

2. THE INSIDE-OUT METHOD

There is more than one approach to the problem of calculating sheath and wake structures. These approaches have in common the following elements. The quantities to be computed include (1) the potential distribution, and (2) the ion and electron density distributions. One may also include the associated surface current densities. The equations to be solved simultaneously are (1) the Vlasov equation for ions, (2) the Vlasov equation for electrons, and (3) the Poisson equation. The solutions of the Vlasov equations (velocity-distribution functions) are used to compute number densities (and surface current densities). The number-density distributions become input to the (right-hand side of the) Poisson equation which yields the potential distribution. Finally, an iterative procedure is used for self-consistency, wherein the density and potential distributions are successively cycled until satisfactory convergence has been achieved.

The steady-state Vlasov equations for ions and electrons state that the velocity distribution functions remain constant along particle trajectories. With the electric field assumed given (numerically in terms of a spatial grid about the body), solving the Vlasov equations means formally that one determines, from the shapes of the trajectories, the ion and electron velocity distributions at the grid points. The trajectories relate local velocities at a given grid point to those at infinity or the surface. Through these relationships, the ion or electron number density at the point may be evaluated by a velocity-integral over the local velocity distribution. Similarly, the current density may be evaluated at desired locations (usually the body surface).

It is convenient to classify various theoretical approaches on the basis of how they treat the trajectory part of the Vlasov problem. An "inside-out" method follows the trajectories backward in time to their source, while an "outside-in" method follows the trajectories forward, in the direction of physical motion of the particles. (In an outside-in method, the velocity-distribution function is not calculated; rather, the density is evaluated directly.) There are in addition other (less realistic) methods involving approximations where trajectories are not followed at all. The three types of approaches are discussed in Parker.[1] There exists as yet no systematic comparison of the results of the various approaches with one another.

For the purposes of discussing the inside-out method, we define here the parameters of interest:

Plasma Parameters

n_o = unperturbed number density at infinity

T_i, T_e = ion, electron temperatures (= T for equal ion and electron temperatures)

m_i = ion mass (electron mass not required)

λ_D = electron Debye length

Body Parameters

R_o = characteristic dimension

v_o = relative velocity of body and plasma

Φ_o = body potential

$\phi_o = e\Phi_o/kT_e$ = dimensionless body potential

M = $v_o\sqrt{m_i/2kT_i}$ = ion Mach number (electron Mach number assumed negligible)

$\lambda_D = \lambda_D/R_o$ = Debye number

Henceforth, all lengths are to be considered normalized by R_o. Thus, λ_D will denote the dimensionless Debye number. We also consider here the case of equal temperatures. Potentials are normalized by kT/e, so that $\phi(\vec{r})$ denotes the dimensionless potential at the spatial point $\vec{r}$. Number densities are normalized by n_o, so that $n(\vec{r})$ denotes the dimensionless density at $\vec{r}$. In the calculations involving integrations over velocities, $\vec{v}$ will denote a velocity normalized by the value of $\sqrt{2kT/m}$ associated with the particles of interest. Similarly, E will denote total energy normalized by kT. Velocity-distribution functions (denoted by f) will be normalized by n_o. For a given body geometry, there are three dimensionless physical parameters of interest, namely, λ_D, ϕ_o, and M. (For unequal temperatures, the temperature ratio T_i/T_e represents an additional parameter.)

Consider a single species of (charged) particle, that is, ions or electrons. The electric field is assumed to be known. In order to compute the number density $n(\vec{r})$ at the point $\vec{r}$, one must evaluate the triple integral over velocity space:

$$n(\vec{r}) = \iiint f(\vec{r}, \vec{v})\, dv_x\, dv_y\, dv_z \qquad (1)$$

where $f(\vec{r}, \vec{v})$ is the distribution function which satisfies the Boltzmann equation for the given species of particle, $\vec{r}$ is the radius vector of the space point of interest, and $\vec{v}$ is the local velocity of a particle at $\vec{r}$. The velocity-volume element is written as if cartesian coordinates were being used, but the product $dv_x dv_y dv_z$ is intended to symbolize an arbitrary coordinate system. Similarly, in order to compute the collected flux at points on the surface of a body, one must evaluate at each point a triple integral over velocity space of the form

$$j(\vec{r}) = \iiint f(\vec{r}, \vec{v})\, v_n dv_x dv_y dv_z \qquad (2)$$

where v_n is the component of the particle velocity normal to the surface at the point $\vec{r}$.

The problem is thus to evaluate f. Since the problems of interest are assumed to be collisionless and constant in time, the distribution function f satisfies the steady-state Vlasov (or collisionless Boltzmann) equation, namely,

$$\vec{v} \cdot \nabla f + \vec{a} \cdot \nabla_v f = 0 \tag{3}$$

where $\vec{a}$ is the vector acceleration of a particle passing with velocity $\vec{v}$ through the point $\vec{r}$. The gradient operators ∇ and ∇_v operate on the components of $\vec{r}$ and of $\vec{v}$, respectively. Equation (3) states that f is constant along a particle orbit, which is characterized by the constants of the motion. In a general electrostatic field (here assumed given) whose sources are volume and surface charges, the total energy E is conserved, where the dimensionless E is defined by

$$E = v^2 + \phi(\vec{r}) \tag{4}$$

and $\phi(\vec{r})$ is the dimensionless potential energy of the particle at $\vec{r}$.

With $\phi(\vec{r})$ a known function of $\vec{r}$, one may evaluate the integrals in Eqs. (1) and (2) by following orbits backward in time with trajectory calculations to a point where f is known. For example, in the case of a body immersed in a plasma, f is assumed to be known at infinity (where ϕ vanishes), and is assumed to have at infinity a prescribed energy distribution, such as a Maxwellian with drift, or a more general distribution. Also, f is assumed to be known on the surfaces of the spacecraft. If a surface emits particles, its distribution function must be prescribed. If the surface absorbs without reemitting charged particles, the distribution function (of emitted particles) is prescribed to be zero. Thus, f is discontinuous in velocity space. That is, the physically-possible velocity space (at the point $\vec{r}$) is divided into three domains, namely, the domain of orbits which have come to $\vec{r}$ from infinity, the domain of orbits which have come to $\vec{r}$ from the spacecraft surfaces, and the domain of trapped orbits (assumed to be unoccupied). The shapes of the boundaries between the domains depend, of course, on the geometry and the potential function ϕ, and it is the heart of the problem (1) to determine the boundaries of the domains of orbits, and (2) to evaluate the integrals Eqs. (1) and (2) over those domains of velocity space.

In practice, one need not in general determine explicitly the boundary of a domain in velocity space. Rather, one may follow a large number of orbits backward in time (computationally), and evaluate the moment integrals, Eqs. (1) and (2), automatically from the results of the orbit-following. It may, however, under some circumstances be more accurate and efficient to determine this boundary. To do so would complicate the computer programming.

For a Maxwellian distribution flowing along the z-direction with Mach number M, the dimensionless velocity-distribution function at infinity may be written:

$$f_o = \frac{1}{\pi^{3/2}} e^{-(v_\infty^2 + M^2 - 2Mv_{z\infty})} = \frac{1}{\pi^{3/2}} e^{-(\phi + v^2 + M^2 - 2Mv_{z\infty})} \qquad (5)$$

(velocities in units of $\sqrt{2kT/m}$,

v_z = axial component of velocity)

where $v_\infty^2 = v^2 + \phi$ may be identified with the total energy E, and $v_{z\infty}$ with $\sqrt{E}$ times the cosine of the angle between $\vec{v}_\infty$ and the axis. A similar Maxwellian distribution may also be used to represent particles emitted from the surface. The moment integral (1) for number density may be approximated by a quadrature sum as follows:

$$n = \iiint \delta f_o \, d^3\vec{v} \simeq \sum_i^I \sum_j^J \sum_k^K A_{ijk} \, \delta_{ijk} \, (f_o)_{ijk} \qquad (6)$$

where $d^3\vec{v}$ is a short-hand notation for the element $dv_x dv_y dv_z$, and δ is a cutoff (or step) function, equal to unity or zero, depending on (1) whether the trajectory is found to come from infinity or the body surface, and (2) whether n represents the density contributed by particles from infinity or from the surface. In the sum, the three indices refer to discrete values of three components of velocity, where the values are chosen in accord with a quadrature scheme (Gaussian), and the coefficients A_{ijk} are proportional to the associated weights and other factors. Each term in the sum represents an individual trajectory. A similar sum is obtained for the flux.

In order to evaluate Eq. (6) for the density, or the corresponding equation for the flux, we transform to energy (E) and angle (α, β) variables in velocity space. We define α and β by:

α = polar angle with respect to z-axis

β = azimuthal angle with respect to the plane containing the z-axis and the point $\vec{r}$.

The angles α and β which define the orientation of the velocity-vector $\vec{v}$ (while $\sqrt{E}$ defines its magnitude) are illustrated in Figure 6.

It is shown by Parker[1] that the integrals for both the density and flux can be transformed to the following form suitable for Gaussian quadratures:

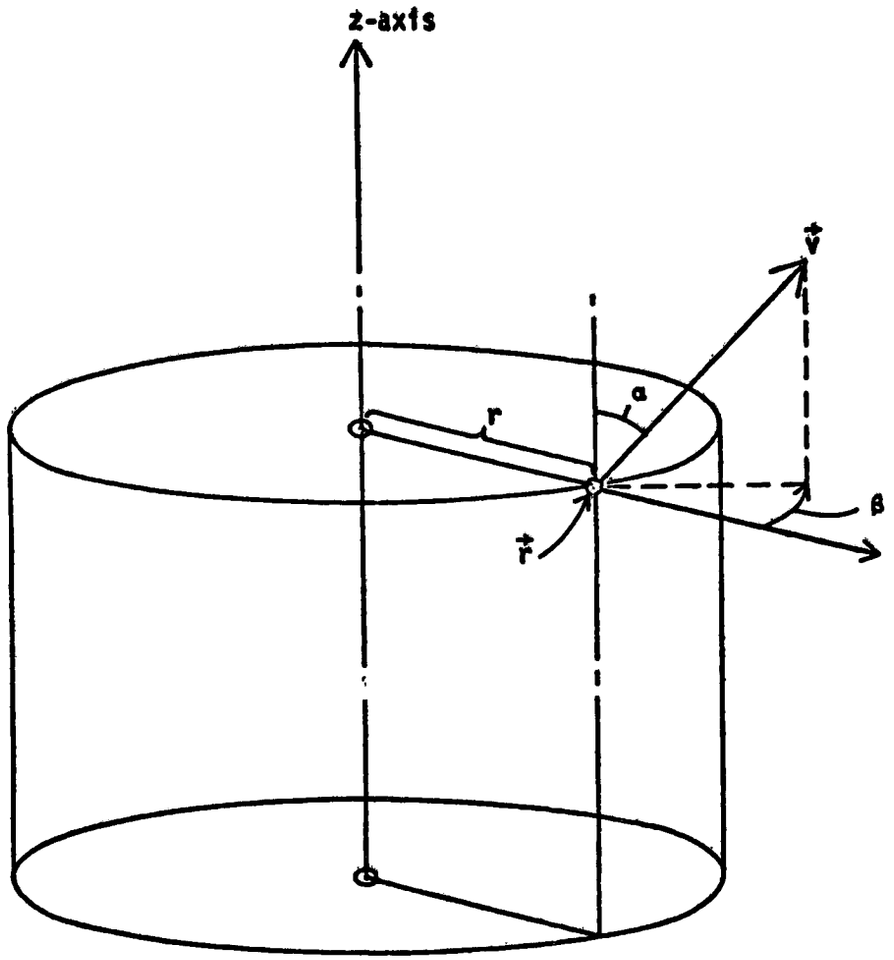

Figure 6. Angle Variables in Velocity Space

$$I = \int_{-1}^{1}\int_{-1}^{1}\int_{-1}^{1} T(a,b,c) \cdot \delta(a,b,c) \cdot da\, db\, dc \quad . \tag{7}$$

Here, the ranges of α, β, and Ë have been transformed to the interval (-1, 1) through the use of new variables a, b, and c. In terms of these latter variables, α, β, and Ë are given by

$$\left.\begin{aligned} \alpha(a) &= \cos^{-1} a \quad \text{for density} \\ \alpha(a) &= \sin^{-1}\sqrt{\frac{1+a}{2}} \quad \text{for flux} \end{aligned}\right\} \tag{8}$$

$$\beta(b) = \frac{\pi}{2}(1 + b) \tag{9}$$

$$E(c) = \frac{1 + c}{1 - c} + \phi_s \tag{10}$$

where the range of α is from 0 to π for density and from 0 to $\pi/2$ for flux; the range of β is from 0 to π; and the range of E is from ϕ_s to infinity, where ϕ_s denotes the potential of the source (infinity or the surface).

The definition of T in the integrand of Eq. (7) is as follows:

$$T(a, b, c) \equiv \frac{e^{-U(a, b, c)}}{(1 - c)^2} \cdot \begin{cases} \sqrt{\dfrac{E(c) - \phi}{\pi}} & \text{for density} \\ \dfrac{E(c) - \phi}{2} & \text{for flux} \end{cases} \tag{11}$$

where U(a, b, c) is given by

$$U(a, b, c) \equiv -\phi_s + E(c) + M^2 + 2M\sqrt{E(c)} \cdot \cos\alpha_\infty(a, b, c) \tag{12}$$

with α_∞ denoting the value of the polar angle of the velocity-vector at infinity, which depends on the local values of α, β, and E (through a, b, and c). The product $\sqrt{E} \cdot \cos\alpha_\infty$ in Eq. (12) is identical to the quantity $v_{z\infty}$ in Eq. (5).

Now it is convenient for flexibility to divide the a-domain into M_a equal subintervals, the b-domain into M_b equal subintervals, and the c-domain into M_c equal subintervals, and then to use Gaussian quadratures of order 2 in each subinterval. This leads to a sum of the following form:[1]

$$I \simeq S \equiv \frac{1}{M_a M_b M_c} \sum_{K_a=1}^{M_a} \sum_{J_a=1}^{2} \sum_{K_b=1}^{M_b} \sum_{J_b=1}^{2} \sum_{K_c=1}^{M_c} \sum_{J_c=1}^{2} T(a';b';c') \cdot \delta(a';b';c') \tag{13}$$

where

$$a' = \frac{1}{M_a}\left(\frac{(-1)^{J_a}}{\sqrt{3}} + 2K_a - 1 - M_a\right)$$

$$b' = \frac{1}{M_b}\left(\frac{(-1)^{J_b}}{\sqrt{3}} + 2K_b - 1 - M_b\right) \tag{14}$$

$$c' = \frac{1}{M_c}\left(\frac{(-1)^{J_c}}{\sqrt{3}} + 2K_c - 1 - M_c\right)$$

Finally, the form of Eq. (6) may be obtained from Eqs. (13) and (14) by writing

$$S = \frac{1}{M_a M_b M_e} \sum_{i}^{I} \sum_{j}^{J} \sum_{k}^{K} T(a_i, b_j, c_k) \cdot \delta(a_i, b_j, c_k) \tag{15}$$

where

$$\left.\begin{aligned} a_i &= a' \quad \text{with } i = J_a + 2(K_a - 1) \\ b_j &= b' \quad \text{with } j = J_b + 2(K_b - 1) \\ c_k &= c' \quad \text{with } k = J_e + 2(K_e - 1) \\ I &= 2M_a \quad J = 2M_b \quad K = 2M_e \end{aligned}\right\} \tag{16}$$

The sum of Eq. (15) consists of 8 $M_a M_b M_e$ terms, each of which represents a trajectory, followed backward from the point of interest. The cutoff function $\delta(a_i, b_j, c_k)$ is zero or unity, depending upon the trajectory defined by the indices i, j, and k characterizing the initial velocity components. The case illustrated in Figure 4 is for contributions from the ambient plasma; for contributions from the surface, δ_{ijk} is zero or unity according as the trajectory reaches infinity or the body surface, respectively.

The computed results to be presented later are based on the assumption of no surface emission.

The method of computation of orbits involves integration of the equations of motion, with the forces given by the components of the gradients of potential. These components are obtained by interpolation between values of potential defined at the points of the grid, say of Figure 3, as described in Parker.[1] The criterion for "escape" or "absorption" of an orbit (that is, evaluation of δ) depends on the geometry of the problem and of the grid. The equations of motion are integrated step-by-step until the orbit either passes out of the outer boundary of the grid ("escapes") or returns to the spacecraft surface (is "absorbed"). The orbit computation time-step is not of physical importance in these time-independent problems where only the shape of the orbit matters. The time-step is kept as large as possible consistent with maintaining the energy loss or gain within desired limits. The method of integrating the equations of motion, the interpolation method to find the forces, and the control of step size, are discussed in Parker.[1]

An important consideration is the accuracy of the quadrature-sum. Naturally, the accuracy is related to the number of terms used, that is, the number of orbits where each term corresponds to a unique orbit. In a test of the energy quadrature alone, and with M = 0, the unperturbed value of density (unity) was computed for

values of M_e = 1, 2, 4, 8, 16, and 32. The corresponding numerical errors were -6 percent, -7 percent, +1.5 percent, -0.05 percent, +0.013 percent, and +0.003 percent. This test was independent of geometry (the α and β integrations were numerically exact). Thus, M_e = 4 (8 values of E) is taken to represent sufficient accuracy (within a few percent) for the purposes of computing density for a Maxwellian distribution without drift (or, for electrons). For large Mach numbers (M) the accuracy of the above unmodified quadrature is diminished. Modification for improving the accuracy at large M by suitably weighting the integrand in the domains of importance are given in Parker. [1]

3. THE POISSON PROBLEM: POISSON DIFFERENCE EQUATIONS

In the present problem the electrostatic field is axially symmetric and is defined on a mesh of spatial grid points, such that at any point (including grid points) the potential and electric field can be obtained by interpolation.

Assume that the space charge density is known at the grid points. Consider a group of interior grid points, forming a portion of the overall grid as shown in Figure 7. In this figure, the vertical and horizontal directions are the z and r directions, respectively, where z and r denote the cylindrical axial and cylindrical radial coordinates, respectively. Three horizontal grid lines, of constant z-values z_{i-1}, z_i, and z_{i+1}, and three vertical grid lines, of constant r-values r_{j-1}, r_j, and r_{j+1}, are shown in the figure. (Note that the index (i) of z increases as z decreases.) The set of grid lines intersect at 9 grid points, or nodes, as shown. Each point may be considered to be associated with a volume of space, and to have a group of four neighboring points which "interact" with it. Thus, consider the central point of the group, labeled C in the figure, which may be identified with one of the grid points in Figure 3. Associated with this point is a volume of revolution (a torus) whose cross-section is rectangular and is shown by the rectangular shaded area surrounding Point C. The shaded area is defined by connecting the midpoints of the surrounding mesh rectangles. Let τ denote the volume of the torus, and let the neighboring points (above, below, to the right of, and to the left of C) be labeled N, S, E and W (north, south, east and west, respectively).

Let the Poisson equation be written in dimensionless form as

$$\nabla^2\phi = -\rho \equiv (n_e - n_i)/\lambda_D^2 \tag{17}$$

where n_e, n_i, λ_D, ϕ and ρ denote the dimensionless electron density, ion density, Debye number, electrostatic potential and space-charge density, respectively, and all lengths are in units of the body radius.

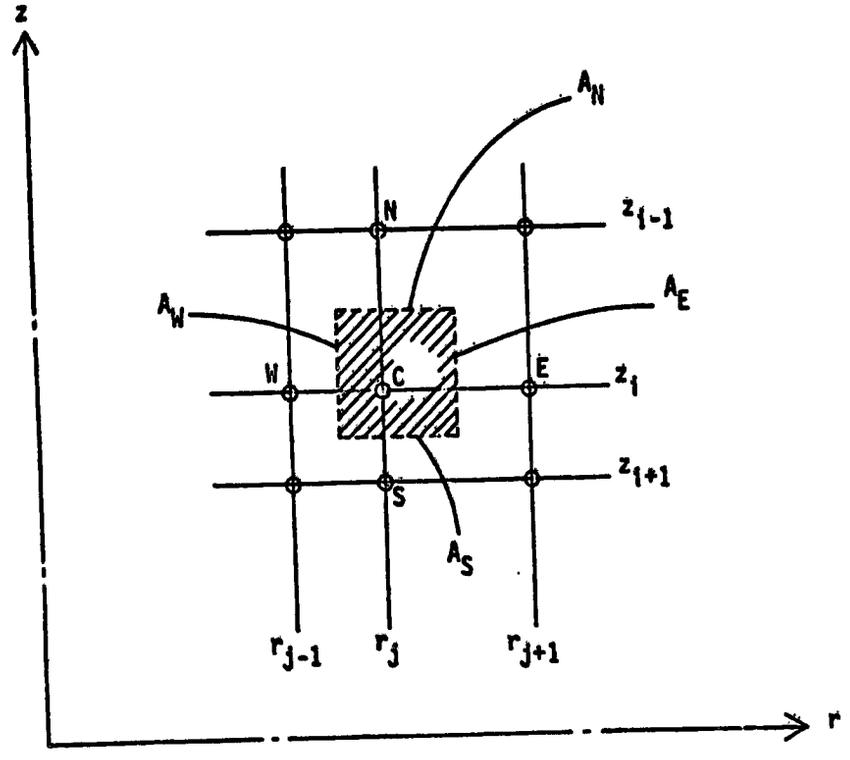

Figure 7. Group of Interior Grid Points in r-z Grid

The grid lines may be considered to be arbitrarily chosen so that the mesh intervals are nonuniform. In this case the Poisson difference equations may be obtained by integrating Eq. (17) over the volume τ of the torus associated with Point C:

$$\iiint_{\tau} \nabla^2 \phi \, d\tau = - \iiint_{\tau} \rho \, d\tau \cong - \rho_C \tau \tag{18}$$

where ρ_C is known at the grid point C. The right-hand side has been approximated as shown since τ is small in principle, and ρ_C is the value of ρ at Point C. By the divergence theorem, the left-hand side becomes

$$\iint_{\Sigma} \frac{\partial \phi}{\partial n} d\Sigma \cong$$

$$A_n \left(\frac{\partial \phi}{\partial n}\right)_N + A_S \left(\frac{\partial \phi}{\partial n}\right)_S + A_E \left(\frac{\partial \phi}{\partial n}\right)_E + A_W \left(\frac{\partial \phi}{\partial n}\right)_W \tag{19}$$

where Σ denotes the surface of the torus; $\partial\phi/\partial n$ is the component of $\nabla\phi$ in the outward normal direction at the surface; A_N, A_S, A_E, and A_W denote the areas of the north, south, east, and west surfaces, respectively; and the quantities $(\partial\phi/\partial n)_{N,S,E,W}$ denote values of $\partial\phi/\partial n$ taken to be constant on the corresponding surfaces.

$(\partial\phi/\partial n)_{N,S,E,W}$ may be approximated by difference quotients, namely,

$$\left(\frac{\partial\phi}{\partial n}\right)_N \cong \frac{(\phi_N - \phi)}{(z_{i-1} - z_i)} \qquad \left(\frac{\partial\phi}{\partial n}\right)_S \cong \frac{(\phi_S - \phi)}{(z_i - z_{i+1})}$$

$$\left(\frac{\partial\phi}{\partial n}\right)_E \cong \frac{(\phi_E - \phi)}{(r_{j+1} - r_j)} \qquad \left(\frac{\partial\phi}{\partial n}\right)_W \cong \frac{(\phi_W - \phi)}{(r_j - r_{j-1})} \tag{20}$$

where ϕ denotes the potential at Point C and ϕ_N, ϕ_S, ϕ_E, ϕ_W denote the neighboring potentials. If Point C is an interior grid point, the areas A_N, A_S, A_E, and A_W are given by

$$\begin{aligned} A_N &= \frac{\pi}{4}\left[(r_{j+1} + r_j)^2 - (r_j + r_{j-1})^2\right] \\ A_S &= A_N \\ A_E &= \frac{\pi}{2}(r_{j+1} + r_j)(z_{i-1} - z_{i+1}) \\ A_W &= \frac{\pi}{2}(r_j + r_{j-1})(z_{i-1} - z_{i+1}) \end{aligned} \tag{21}$$

and the volume τ is given by

$$\tau = \frac{A_N}{2}(z_{i-1} - z_{i+1}) \quad . \tag{22}$$

Thus we obtain the difference equation in the form

$$C_N\phi_N + C_S\phi_S + C_E\phi_E + C_W\phi_W - C\phi = -\rho_C\tau \tag{23}$$

where

$$C = C_N + C_S + C_E + C_W \tag{24}$$

and

$$C_N = \frac{A_N}{(z_{i-1} - z_i)} \qquad C_S = \frac{A_S}{(z_i - z_{i+1})}$$

$$C_E = \frac{A_E}{(r_{j+1} - r_j)} \qquad C_W = \frac{A_W}{(r_j - r_{j-1})} \tag{25}$$

This shows how to form the difference equations used for the Poisson problems of this paper. Equation (24) holds only for an "interior" point of the grid, that is, a point surrounded by neighbors on all four sides. If Point C has a known neighboring potential (for example, if Point C is adjacent to the spacecraft surface), then the corresponding term on the left-hand side of Eq. (23) is transferred to the right-hand side as a known quantity.

The boundary conditions for the potentials in the Poisson problem are as follows. At points representing the body surface, the normalized potentials are fixed at the chosen values. At the external (boundary) points of the grid, where "infinity" is represented on the computer, a "floating" condition is optionally used, namely, a linear relation between ϕ and $\partial\phi/\partial n$, the normal component of $\nabla\phi$. The exact relation of ϕ to $\partial\phi/\partial n$ is not important when the external boundary of the grid is sufficiently far away. (For the calculations to be reported, the assumed relation was the same as for a Coulomb potential.) In any case, either the fixed condition $\phi = 0$ or the floating condition will give the same results, provided the grid boundary is moved sufficiently far out. The effect of various types of boundary conditions representing "infinity" have been studied by Taylor[12] and by Parker and Sullivan.[8] In general, the floating condition appears to be computationally more efficient than the fixed one. Of course, the floating condition becomes ideal when the true relation between ϕ and $\partial\phi/\partial n$ is used, but this requires that the asymptotic form of the solution be known in advance. For example, see Parker and Whipple.[14] The boundary conditions at the outer grid surfaces can be combinations of fixed and floating conditions.

Consider a Point C on the outer boundary of the grid where a floating boundary condition is chosen. If the potential is assumed to satisfy the linear law

$$\frac{\partial\phi}{\partial n} = \frac{\partial\phi}{\partial z} = -\alpha\,\phi \tag{26}$$

on the z-boundary (North or South), and

$$\frac{\partial\phi}{\partial n} = \frac{\partial\phi}{\partial r} = -\beta\,\phi \tag{27}$$

on the r-boundary (East only; $\beta=0$ on the West), then the corresponding "neighbor term" on the left-hand side of Eq. (23) vanishes, and the corresponding "neighbor coefficient" on the right-hand side of Eq. (24) is replaced by αA or βA, where A is the appropriate area. The quantities α and β depend on the position and on the assumed model for the variation of the potential at large distances.

Once the coefficients of all of the equations (corresponding to the grid points where the potentials are unknown) are computed, the system of linear equations of the form of Eq. (23) may be solved by iteration. Point-successive over-relaxation is a well-known process and has been found to be effective in the present problem. For the relaxation process, one rearranges the equations, so that the "diagonal" term is alone on the left-hand side, while all the other terms are on the right-hand side with the known charge-density term. Thus, Eq. (23) becomes

$$C\phi = C_N\phi_N + C_S\phi_S + C_E\phi_E + C_W\phi_W + \rho_C\tau \quad . \tag{28}$$

First, an initial guess is made for the values of all the potentials. Then new values are obtained from the left-hand sides of all of the equations (28), using previous values on the right-hand sides. One "sweeps" through the equations successively, replacing the potentials on the right-hand sides with updated values as they become available from preceding equations. This procedure is usually stable and leads to convergence. "Over-relaxation" is the process of mixing successive potential iterates in such a way as to enhance the rate of convergence. [1]

When the potential distribution is such that the electron density n_e is approximable by the Boltzmann factor $\exp(\phi)$, the relaxation equations (28) can include the electron density as an unknown function on the left-hand side. The equations are then nonlinear; they may be solved for ϕ by a Newtonian process, with the ion density n_i considered fixed. This procedure is promising for large-body problems.[1]

4. SAMPLE RESULTS APPLIED IN IN-SITU DATA

The calculations reported here refer to two in-situ experiments, Ariel 1[15] and Explorer 31[16], where data are available. These results are preliminary in that they are intended as an illustration of the capability of the program rather than as a systematic study. Geometrically, the body is assumed to be a pillbox, a cylinder of height equal to its diameter. The three dimensionless physical parameters defining the problem are ϕ_o, M, and λ_D, defined (earlier) by:

$$\phi_o = e\Phi_o/kT$$

$$M \equiv mv_o^2/2kT$$

$$\lambda_D \equiv \underline{\lambda}_D/R_o$$

where T is the plasma temperature (assumed to be the same for ions and electrons), ϕ_o is the body potential (for a conducting nonemitting body), v_o is the velocity of the plasma flow relative to the body and parallel to its axis, m is the ion mass, R_o is the body radius, and $\underline{\lambda}_D$ is the dimensional Debye length.

The numerical parameters for the calculations to be described include of the order of 100 grid points, distributed mostly in the wake region, and of the order of 500 trajectories per grid point, distributed among the two angles and the energy.

4.1 Ariel-I Satellite

Figure 8 is a schematic drawing of the Ariel 1 satellite, showing the location of electron and ion probes, after Henderson and Samir.[15] The boom-mounted

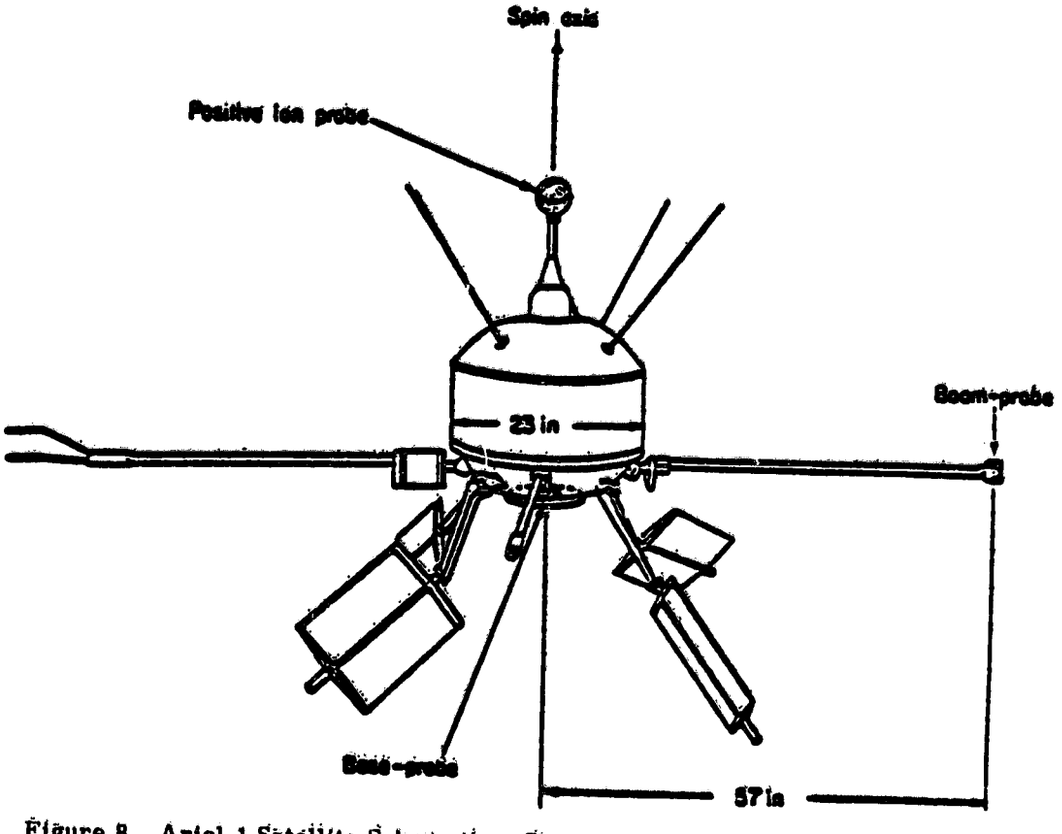

Figure 8. Ariel 1 Satellite Schematic. Shows main body, positive-ion probe, and electron boom-probe

probe measures electron currents at a distance 5 R_o from the center of the satellite (main body) which has a radius R_o = 11.5 in or 29 cm. The ion probe mounted near the surface and on the spin axis is a small sphere 6.6 times smaller than the main body. The satellite velocity is such that the ion Mach number is about 4. The satellite potential is about 4 kT (1 volt) negative with respect to space. The satellite radius is equal to about 10 Debye lengths. Due to the satellite motion, spin, and orientation, the boom probe sweeps through the wake during each spin revolution. In successive revolutions, it sweeps through at different angles and samples the structure of different parts of the wake.

Figure 9 shows normalized electron current data taken from the paper by Henderson and Samir (their figure 4).[15] In particular, the data at $\theta = 84^o$ (labeled "MAIN") samples the wake structure associated with the main body, while the data at $\theta = 60^o$ (labeled "I. P.") samples the wake structure of the ion probe. We will consider separately the main body and ion probe in the following comparisons between the data and theoretical calculations.

4.1.1 ARIEL 1 MAIN BODY

Although the data in Figure 9 is "bumpy," the $\theta = 84^o$ profile for the main body indicates a minor central peak or bump, of height about 80 percent of ambient, within the depleted wake region where the minimum is about 50 percent of ambient.

Figure 10 shows transverse profiles computed for the wake of the main body, of n_i (normalized ion density), n_e (normalized electron density), and ϕ (dimensionless potential) in the wake region downstream. The parameter values in Figure 10 are $\phi_o = -4$, $M = 4$, $\lambda_D = 1/10$. Thirteen major iterations (Poisson-Vlasov cycles) were computed. The profiles are in transverse planes at various distances downstream, and all lengths are normalized by the body radius. Thus, z denotes axial distance downstream, in radii, with $z = 0$ defined as the rear surface of the pillbox (looking into the wake); and r denotes radial or transverse distance from the axis ($r = 1$ is the body radius). The profiles of n_i, n_e, and ϕ are arranged vertically in order of increasing axial distance z. There are 8 values of z, namely, $z = 0.2$, 0.5, 1.0, 2.0, 3.0, 4.0, 5.0, and 6.0. Each profile is constructed of 9 values of r, namely, $r = 0$, 0.1, 0.3, 0.6, 0.8, 1.0, 1.2, 1.5, and 2.0. The outer-boundary conditions are applied at $z = 6$ and $r = 2$; for the main-body problem, the boundary condition at $z = 6$ is the fixed one, while floating conditions are used elsewhere. The profiles consist of straight-line segments connecting the values of the functions (n_i, n_e, or ϕ) computed at 72 grid points in the wake region.

The features of the wake structure are as follows. The near wake ($z < 1$) is clearly depleted of both ions and electrons, with the ion density lower than the electron density. Further downstream the wake becomes increasingly filled in, between about $z = 1$ and $z = 4$, where $z = 4$ is the ion-Mach-number of radii

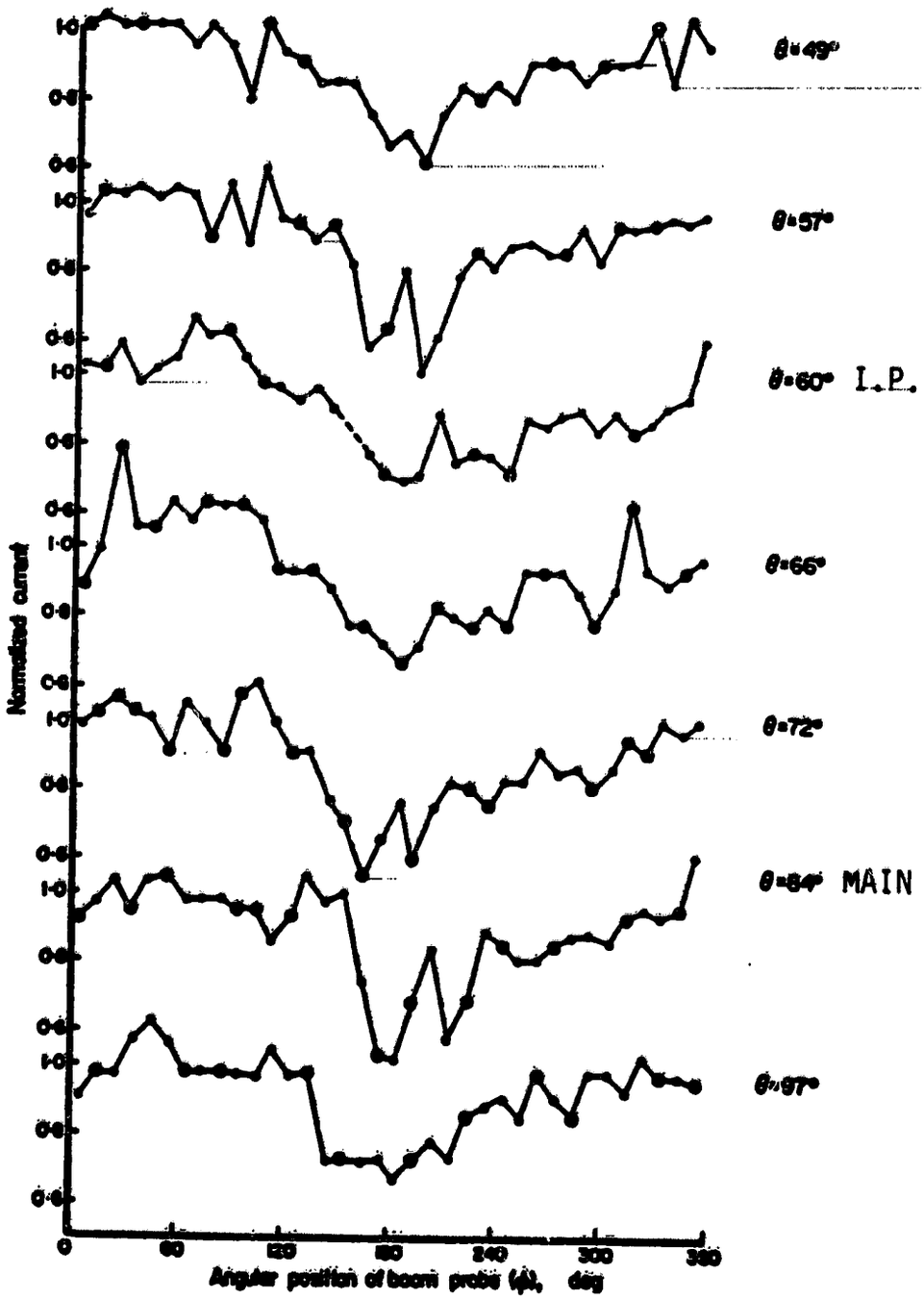

Figure 9. Normalized Electron Current versus Angular Position of the Boom Probe, for Various Spin-Orientation Angles

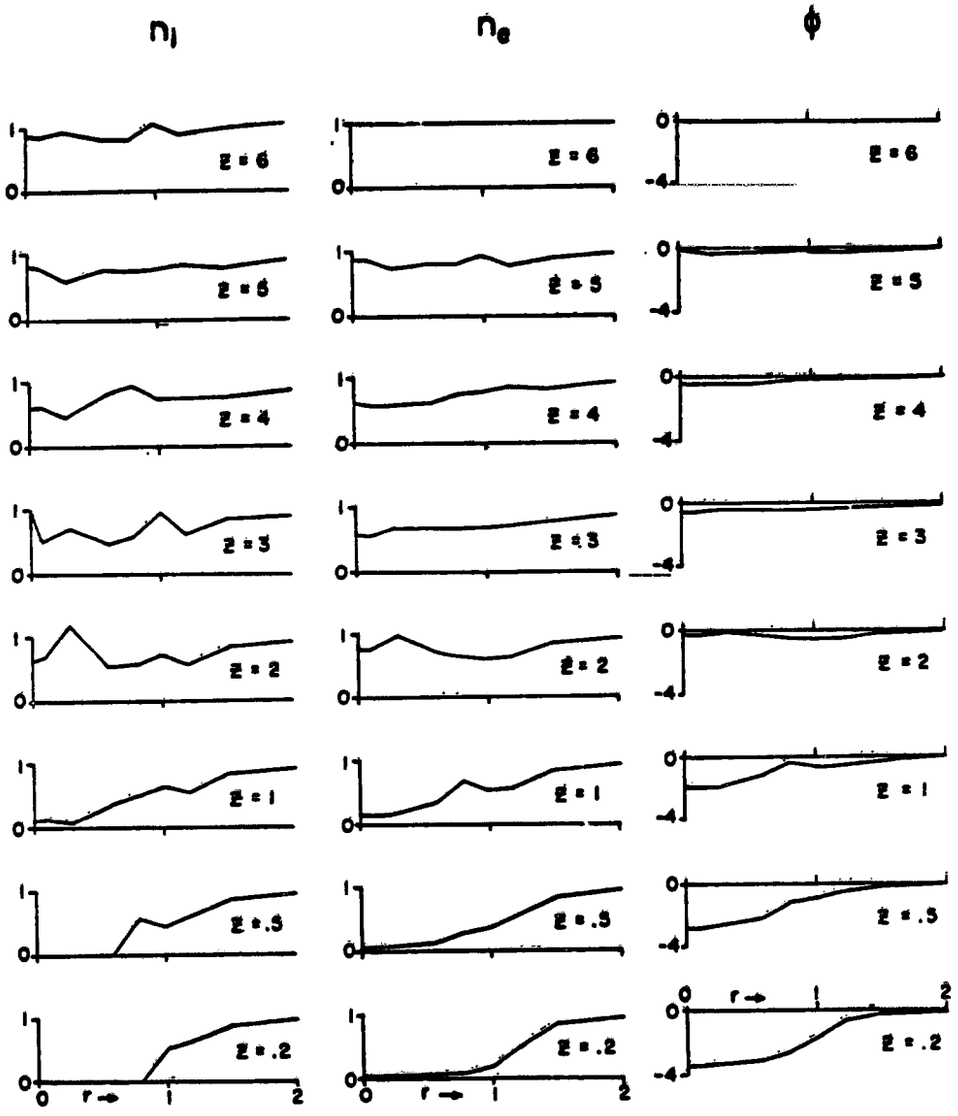

Figure 10. Ariel 1 Main Body Wake Profiles. $\phi_o = -4$, M = 4, $\lambda_D = (10)^{-1} = 0.1$

downstream. In this range of z the ion profiles tend to be relatively noisy, indicating sensitivity to numerical errors, which may in turn imply a tendency toward physical instability. The trend of the ion and electron profiles suggests a radially-inward bulk motion of the plasma within the wake as if it were a fluid wave propagating inward, piling up near the center, and bouncing out again as it moves downstream. The disturbance has essentially died away at z = 6 radii downstream.

There is no well-defined central bump similar to that in the experimental data in Figure 9.

4.1.2 ARIEL 1 ION PROBE

According to Henderson and Samir the profile in Figure 9 at $\theta = 60^{\circ}$ samples the ion probe wake structure. This structure is similar to that of the main body, having a below-ambient central peak within a depleted region of about the same width as that associated with the main body. The ion probe is about 1.7 Debye lengths in radius and is biased at about 28 kT (7 volts) negative with respect to space. Hence it may be expected to produce at least a pronounced focusing effect, as is borne out by the following computed results.

Figure 11 shows transverse profiles computed for the wake of the ion probe. The notation is the same as that of Figure 10. The parameter values are $\phi_o = -28$, $M = 4$, and $\lambda_D = 1/1.7$. Ten major iterations were computed. The outer boundary at $z = 10$ was placed sufficiently far downstream to ensure that the disturbances of interest are contained within the grid. Moreover, a floating condition is employed there as well as elsewhere. (The number of grid points was larger than in the main-body problem.)

The main features are as follows. The ion profiles at $z = 1$ and $z = 2$ show that a strong focusing effect occurs near the body. Further downstream, however, the disturbance dies out; there is essentially none at $z = 8$ and beyond.

The radially-inward and outward bulk motion of the plasma as it fills the wake is again a fluid-like feature. Again, there is no persistent peak at the center of the wake as indicated by the data. If this were an isolated body, the Henderson-Samir data would imply that the peak persists far downstream to beyond a distance of 33 radii. The present theoretical calculation indicates no structure at $z = 8$ and beyond.

4.1.3 COMMENT ON COMPARISON OF THEORY WITH EXPERIMENT

A central bump may perhaps be generally expected on the basis of nonrigorous theoretical arguments invoking (1) electrostatic focusing effects or (2) convergence of ion streams during the filling of the wake principally at a Mach number of radii downstream, or (3) a combination of these.[15] However, previous theoretical calculations indicating such bumps have been deficient in some respect with regard to their rigorous applicability (for example, cold ions, infinitely-long cylinders, non-self-consistent). Similarly, there have been laboratory-simulation experiments which have indicated bumps.[17] However, it is presently still difficult to simulate ion transverse velocity distributions in the laboratory, and the effective ion temperature is generally too low. Hence, there does not exist thus far an unambiguous explanation of the Ariel 1 data. (Note: T_i was not measured, but was assumed here to be equal to T_e. Theoretically, bumps in the wake have been predicted for T_i less than T_e.[11,18])

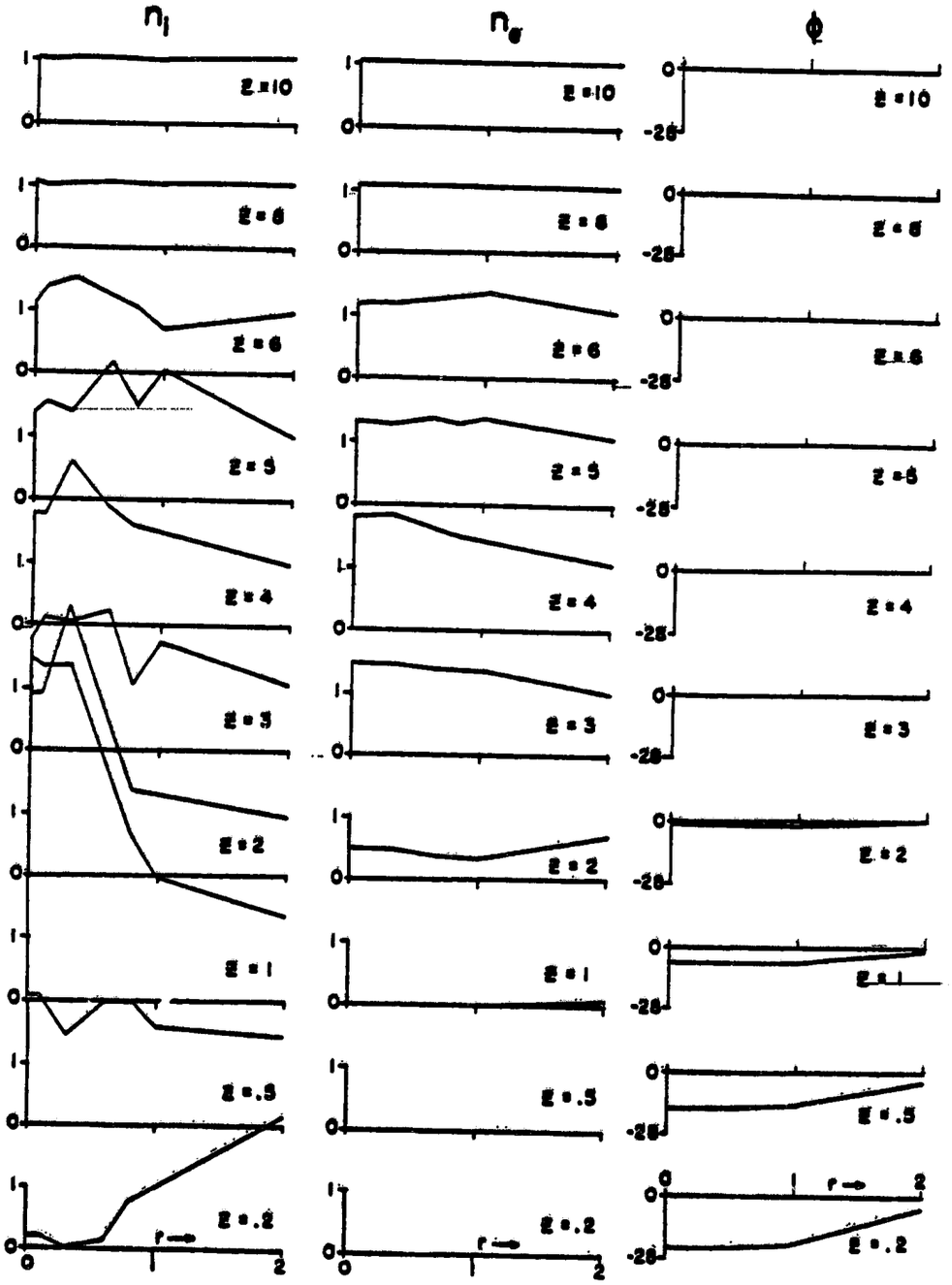

Figure 11. Ariel 1 Ion Probe Wake Profiles. $\phi_o = -28$, M = 4, $\lambda_D = (1.7)^{-1} = 0.6$

It is also of interest to note that a large body produces a central-core enhancement, as will be shown later.

4.2 Explorer 31 Satellite

The results of this section were obtained in the process of computing a number of solutions to be compared with in-situ data obtained on the Explorer 31. The parameters adopted were suggested by Samir (private communication) based on 8 different passes of the Explorer 31 satellite, as listed in his paper with Jew.[16] A small portion of two of these cases will be discussed here, without a quantitative comparison with data, in order to illustrate a specific point.

Figure 12 shows computed electron and ion density transverse profiles in the very near wake of a body with the parameters

$$\phi_o = -4.3$$
$$\lambda_D = (6.9)^{-1}$$
$$M = 3.4 \ .$$

These are the parameters in the case of Curve No. 1 of Samir and Jew.[16] The computed profiles in Figure 12 are at z = 0.2 radii downstream, that is, similar to the lowest profiles in Figure 10 where the parameters are of similar order. Here the vertical scale (normalized density) is logarithmic, as opposed to Figure 10, where it is linear. The ion densities are denoted by circles and the electron densities by squares. The principal features shown in Figure 12 are as follows. For r greater than about 0.8 radii, the ion density is higher than the electron density. Moreover, the ion density drops more abruptly in the vicinity of the "shoulder" ($r \cong 1$) than the electron density. In the central wake both densities are far below normal, with the ion density about an order of magnitude below the electron density. This is the usually-expected picture of near-wake structure.

Figure 13, on the other hand, shows corresponding computational results for the case of Curve No. 4 of Samir and Jew,[16] where the parameters are:

$$\phi_o = -5.4$$
$$\lambda_D = (3.1)^{-1}$$
$$M = 1.1 \ .$$

Here, the most significant change is the lower Mach number (1.1). The curves in Figure 13 are qualitatively different from those in Figure 12. The new electron density profile is shifted downward slightly, but the new ion density profile is moved up to approximately a constant roughly equal to the normal value.

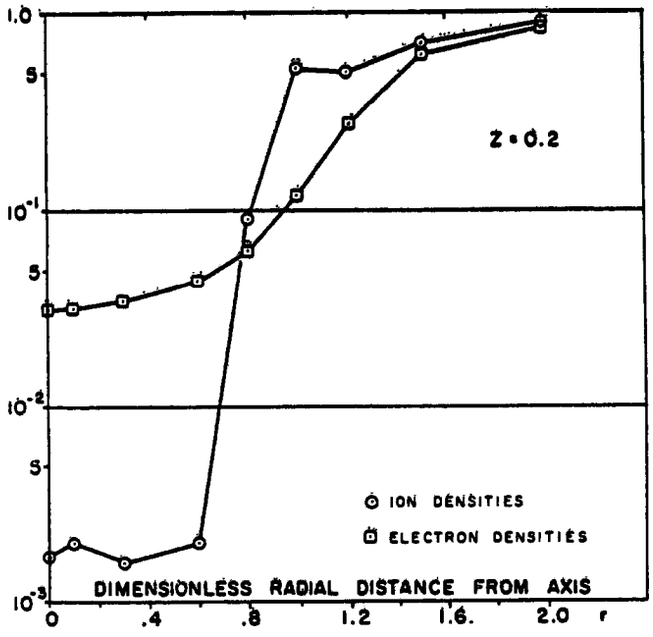

Figure 12. Explorer 31 Density Profiles, Case 1. $\phi_o = -4.3$, $M = 3.4$, $\lambda_D = (6.9)^{-1} = 0.145$

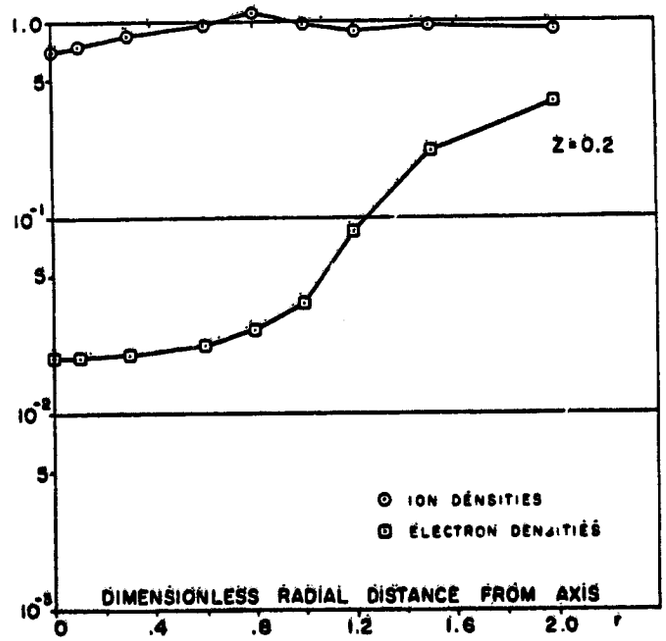

Figure 13. Explorer 31 Density Profiles, Case 4. $\phi_o = -5.4$, $M = 1.1$, $\lambda_D = (3.1)^{-1} = 0.32$

The fact that the ion wake density is above the electron density at all r may be unexpected from the point of view of "traditional" wake theory, but seems reasonable on the basis of Langmuir probe theory.[2-5] According to probe theory, a stationary negative electrostatic probe in a plasma will have adjacent to it a sheath in which the ion density exceeds the electron density. If the probe begins to move slowly relative to the plasma, one expects the sheath structure at first to be only slightly changed, with a continuation of the predominance of the ions over the electrons. At sufficiently large velocity, however, the traditional wake structure with electron domination over ions should appear as in Figure 12. The value of ion Mach number at which the transition should occur has not been predicted but can be established by additional computations of the present type.

5. A LARGE-BODY PROBLEM

In this section we consider the wake of a large body, 100 Debye lengths in radius.[1] The body is in the form of a disk oriented normal to the flow. For this case (Figures 14 and 15) the parameter values are

Figure 14	Figure 15
$\phi_o = -4$	$\phi_o = -4$
$\lambda_D = (100)^{-1}$	$\lambda_D = (100)^{-1}$
$M = 4$.	$M = 8$.

Here the parameter values differ qualitatively from those of the preceding problems in that λ_D is so small. This size of moving body is larger than has been previously treated by trajectory-following, that is, realistic, calculations. The results show what may be expected for the wake structure of large bodies in general. This case requires more effort (computer time and judicious selection of numerical parameters) than that of a smaller body. The solutions shown, therefore, are intended to be illustrative rather than accurate.

Six iterations, or Poisson-Vlasov cycles, were computed using the ion-density option, in which successive iterates were not mixed, starting with the neutral ion density as an initial guess. The nominal number of trajectories, 512, was used at all grid points.

The profiles of n_i, n_e, and ϕ in Figure 14 are constructed in the same way and at the same grid points as in Figure 10. Tabulated values are given in Parker.[1] The wake is essentially "empty" of both ions and electrons between $z = 0$ and $z = 1$, and begins to fill up between $z = 2$ and $z = 3$. In this way, the wake is qualitatively similar to that in Figure 10.

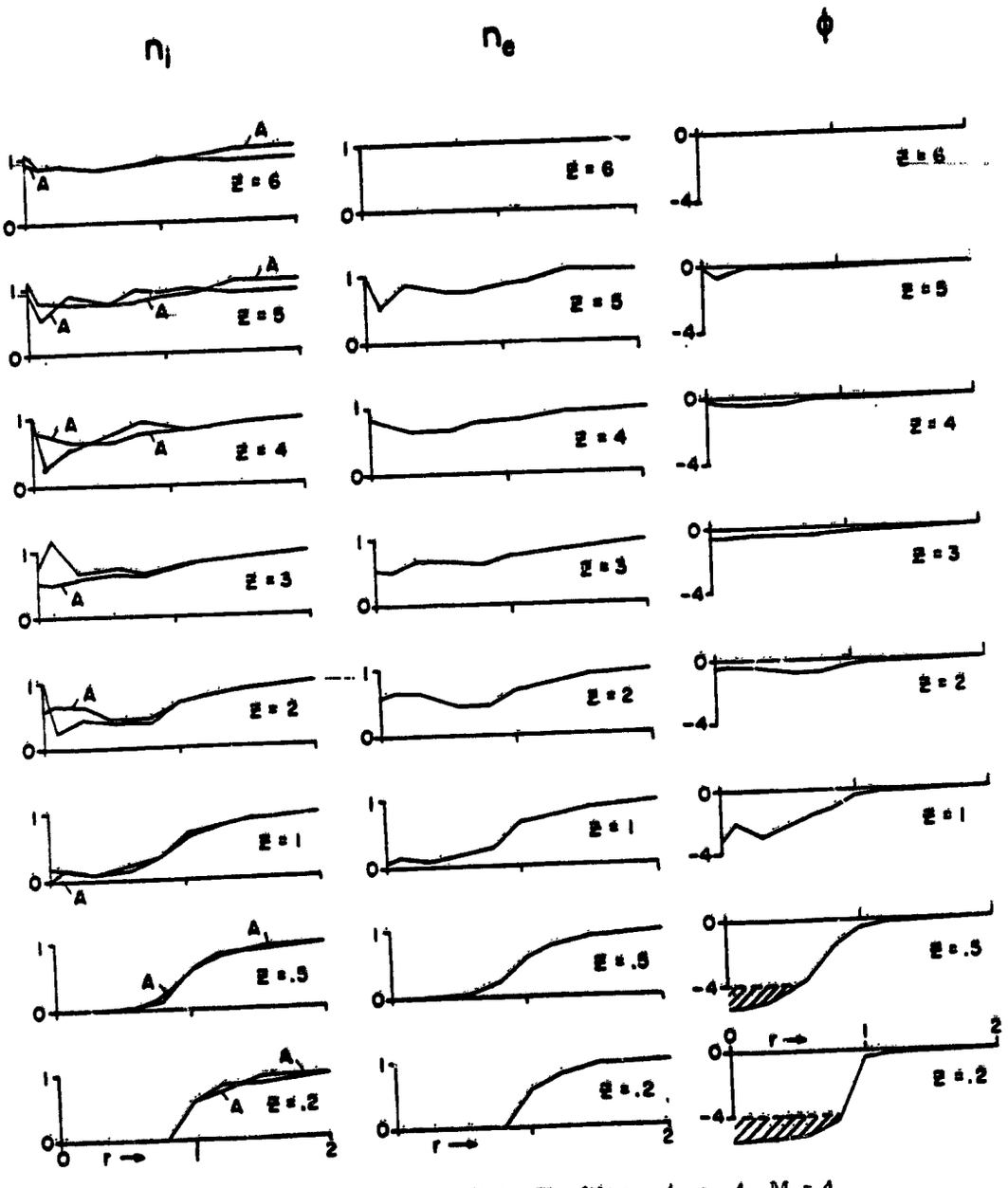

Figure 14. Large-Body Wake Profiles. $\phi_o = -4$, M = 4, $\lambda_D = (100)^{-1} = 0.01$

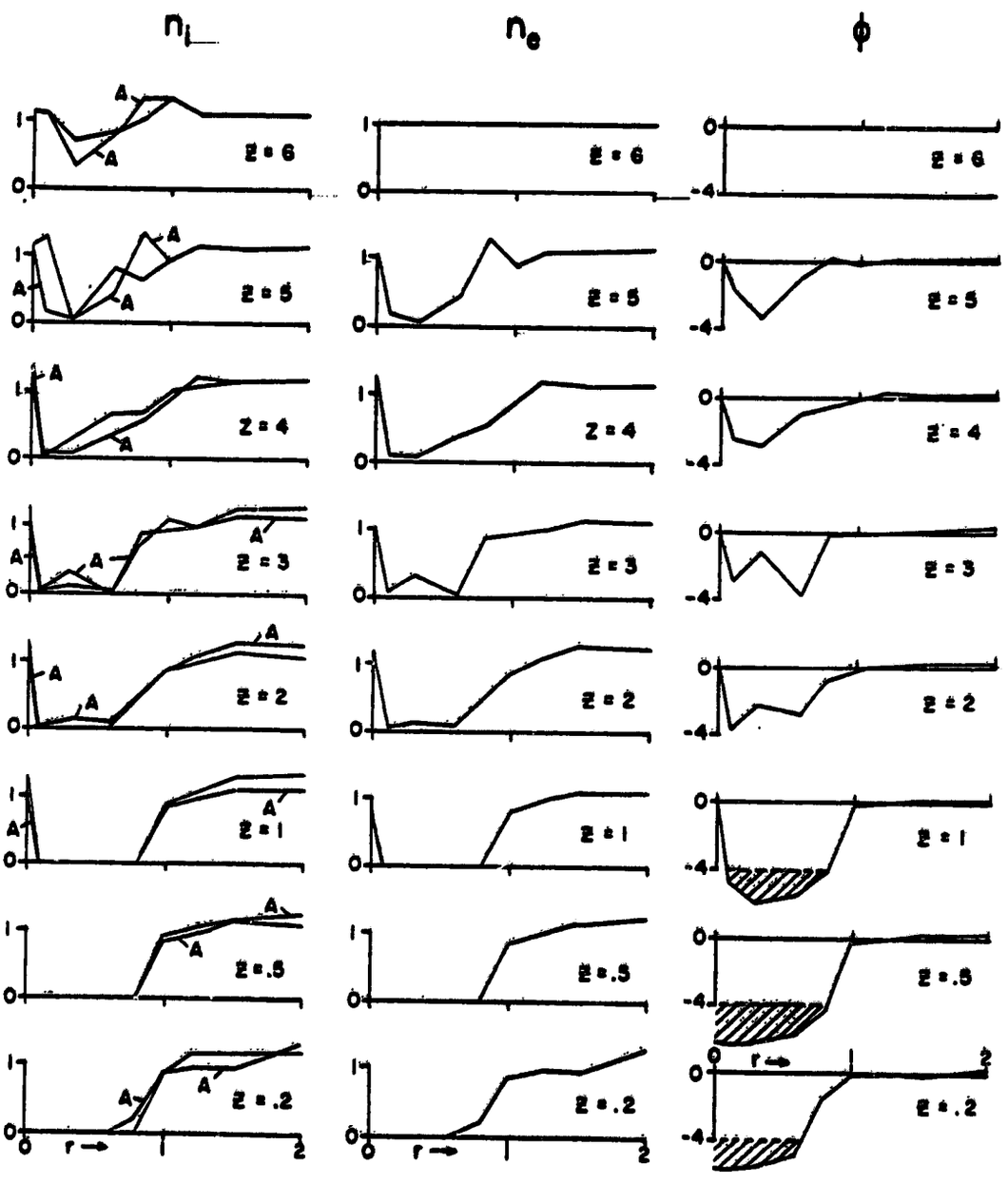

Figure 15. Large-Body Wake Profiles. $\phi_o = -4$, M = 8, $\lambda_D = (100)^{-1} = 0.01$

Two sets of ion-density profiles are shown on the left side of Figure 14, the unlabeled profiles for the 6th order (6th iteration), and the profiles labeled "A" for the 5th order. Comparison of the n_e-profiles with the 5th order n_i-profiles (labeled "A" to denote that the ϕ-profiles and n_e-profiles in the figure are derived from these) indicates that the quasineutrality assumption is valid everywhere outside a cone-shaped region near the wake surface; the cone height along the axis is between 1 and 2 radii. This is in accord with expectation for a large body. Near the wake surface, however, quasineutrality is violated because the effective Debye length is large. The similarity of the n_i-profiles (labeled "A") and the n_e profiles in Figure 14 is a consequence of near-quasineutrality.

Comparison of the 5th and 6th order n_i-profiles (labeled "A" and unlabeled) in Figure 14 show that the solution is reasonably converged for $z = 1$ and below, but that there is incomplete convergence at $z = 2$ and beyond. The incomplete convergence and apparent structure at $z = 2$ and beyond may be artifactual due to insufficient numerical accuracy. (No attempt was made to achieve high accuracy since this was regarded as a preliminary run.) The structure and lack of convergence are seen to extend past $z = 5$, so that the downstream boundary should be placed further than at $z = 6$.

Despite possible inaccuracies, one may infer additional physical conclusions indicated by Figure 14, namely, (1) the suggestion of a core of high (approximately ambient) density of ions and electrons on the axis, and (2) the occurrence of a potential well in the near wake, defined as a region with ϕ-values below -4. The shading in the two lowest ϕ-profiles denote cross-sections of this well. The wake-surface normalized fluxes are 1.1×10^{-8} (5th order) and 2.4×10^{-7} (6th order) for ions, and 4.3×10^{-3} for electrons. The electron current density is less than exp(-4), as would be expected in the presence of a potential well.

The region of wake disturbance probably extends more than 6 radii downstream, and between 2 and 3 radii in the transverse direction.

Another large-body case (Figure 15) is similar to the previous large-body case except that the Mach number is increased from $M = 4$ to $M = 8$. Ten iterations were computed in which successive iterates were used without mixing, starting with uniform ambient ion density. (The latter starting condition was inadvertently different from that of the $M = 4$ calculation which was started with the neutral ion density, but this difference should become unimportant after many iterations.) Similar statements may be made about the incompleteness of the convergence as in the $M = 4$ case. The 9th and 10th order ion densities are labeled "A" and unlabeled, respectively. On comparing these, the convergence seems fairly good at $z = 0.5$ and $z = 1$. Again, the disturbance extends beyond $z = 5$, so that the downstream boundary should be moved further than $z = 6$.

Despite inaccuracies, the consistency is such that physical conclusions may be drawn as follows. In this case, the wake is seen to remain empty further downstream than in the M = 4 case. In addition, the suggestion is much stronger that there is a central core of ambient density for both ions and electrons along the axis. Moreover, the potential well is wider and longer than in the M = 4 case, although the depth is about the same. The normalized wake-surface fluxes are 7.4×10^{-30} (9th order) and 4.2×10^{-30} (10th order) for ions, and 3.7×10^{-3} for electrons. The electron flux is slightly less than the M = 4 value, and is again less than exp(-4).

The conical region behind the disk where quasineutrality breaks down is now longer than in the M = 4 case, extending to between z = 4 and z = 5 along the axis.

The region of wake disturbance is probably longer than 6 radii downstream, as in the M = 4 case, but may not extend beyond about 2 radii in the transverse direction.

Acknowledgment

The author wishes to thank the National Aeronautics and Space Administration for its support of this work.

References

1. Parker, L. W. (1976) Computation of Collisionless Steady-State Plasma Flow Past a Charged Disk, NASA CR-144159, Lee W. Parker, Inc.
2. Parker, L. W. (1976) Theory of Electron Emission Effects in Symmetric Probe and Spacecraft Sheaths, AFGL-TR-76-0294, Final Report, Lee W. Parker, Inc.
3. Parker, L. W. (1975) Computer Method for Satellite Plasma Sheath in Steady-State Spherical Symmetry, AFCRL-TR-75-0410, Final Report, Lee W. Parker, Inc.
4. Parker, L. W. (1973) Computer Solutions in Electrostatic Probe Theory, AFAL-TR-72-222, Final Report, Mt. Auburn Research Associates, Inc.
5. Laframboise, J. G. (1966) Theory of Spherical and Cylindrical Langmuir Probes in a Collisionless Maxwellian Plasma at Rest, UTIAS Report No. 100.
6. Parker, L. W. (1964) Numerical Methods for Computing the Density of a Rarefied Gas About a Moving Object, AFCRL-64-193, Allied Research Associates, Inc.

7. Parker, L. W. (1970) Theory of the External Sheath Structure and Ion Collection Characteristics of a Rocket-Borne Mass Spectrometer, AFCRL-71-0105, Mt. Auburn Research Associates, Inc.

8. Parker, L. W., and Sullivan, E. C. (1974) Iterative Methods for Plasma-Sheath Calculations, NASA TN D-7409.

9. Call, S. M. (1969) The Interaction of a Satellite with the Ionosphere, Columbia Univ. Report No. 46.

10. Fournier, G. (1971) Collisionless Plasma Flow Around a Cylinder Considering Applications to Ionospheric Probes (in French), O. N. E. R. A. Publication No. 137, Paris.

11. Martin, A. R. (1974) Numerical solutions to the problem of charged particle flow around an ionospheric spacecraft, Planet. Space Sci. 22:121-141.

12. Taylor, J. C. (1967) Disturbance of a rarefied plasma by a supersonic body on the basis of the Poisson-Vlasov equations, Planet. Space Sci. 15:155-187.

13. Grabowski, R., and Fischer, T. (1975) Theoretical density distribution of plasma streaming around a cylinder, Planet. Space Sci. 23:287-304.

14. Parker, L. W., and Whipple E. C., Jr. (1970) Theory of spacecraft sheath structure, potential, and velocity effects on ion measurements by traps and mass spectrometers, J. Geophys. Res. 75:4720-4733.

15. Henderson, C. L., and Samir, U. (1967) Observations of the disturbed region around an ionospheric spacecraft, Planet. Space Sci. 15:1499-1513.

16. Samir, U., and Jew, H. (1972) Comparison of theory with experiment for electron density distributions in the near wake of an ionospheric satellite, J. Geophys. Res. 77:6819-6827.

17. Oran, W. A., Stone, N. H., and Samir, U. (1975) The effects of body geometry on the structure in the near wake zone of bodies in a flowing plasma, J. Geophys. Res. 80:207-209.

18. Gurevich, A. V., and Dimant, Ya. S. (1975) Flow of a rarefied plasma around a disk, Geomagn. Aeron. (USSR, Engl. Transl.) 15:183-190.